www.rericjournal.ait.ac.th

Analyses of Absorber Tube of Parabolic Trough Solar Collector (PTSC) based on Convective Heat Transfer Coefficient of Fluid

Hamzeh Jamali*[1]

Abstract – In this article, analyses of a PTSC absorber tube are carried out comparing three modes of a PTSC, which are PTSC with: 1) plain smooth absorber tube, 2) plain enhanced absorber tube 3) absorber tube with vacuum glass tube. For this, a PTSC of a solar power plant situated in Shiraz, Iran is considered as the article reference model. In the paper, the influence of convective heat transfer coefficient of fluid on thermal efficiency of PTSC is analyzed for the three different modes mentioned above, regarding the heat losses. In addition, the dimensionless numbers Nusselt, Reynolds, and Prandtl are used within formulas and diagrams to help the analyses. Finally, it is numerically and graphically shown how the integration of the second and third modes of PTSC will increase PTSC thermal efficiency in comparison with the first mode of PTSC.

Keywords – Absorber tube, convective heat transfer, enhancements, friction, solar.

1. INTRODUCTION

Since one of the most essential efforts made by many scientists and technologists towards renewable energy systems improvement is to develop solar energy throughout the world as an alternative energy which is environmentally friendly, this paper aims at improving utilization of solar energy by analytically discussing the ways to raise the thermal efficiency of PTSC through convective heat transfer coefficient of the relevant fluids. For this, a PTSC unit of a solar power plant situated in Shiraz, Iran (specifications in Table 1) is selected to be investigated in this paper, helping in terms of model and data. As a PTSC produces electricity thermally through heating oil (VP-1 oil in this research) flowing in an absorber tube positioned at the focal point of PTSC, the influence of convective heat transfer coefficient of fluid on thermal efficiency of PTSC takes on great importance and is mainly discussed in this article. Among the factors on which PTSC thermal efficiency depends the fluid flow inside the absorber tube and the air flow outside it play important roles. For this, the article focuses on the convective heat transfer coefficients of the fluid inside absorber tube and the air around it. Three important modes of PTSC absorber tube that are: plain smooth absorber tube, plain enhanced absorber tube, and absorber tube with vacuum glass tube are studied. As well, the effects of the absorber tube internal friction factor and also the swirl-induced mechanisms as the absorber tube internal enhancements on the convective heat transfer coefficient of working fluid are considered and discussed within the article analyses. The dimensionless numbers Nusselt, Reynolds, Prandtl are mainly used in this article to help carry out this analysis. Many functions are applied and plotted using MATLAB software so that the diagrams help understand the analyses.

Table 1. Specifications of a unit of the studied PTSC.

Absorber tube inner diameter (D_i)	6.56 cm
Collector aperture area (A_a)	25 m * 4.3 m
Emissivity of absorber tube (ε)	0.15
Emissivity of pyrex glass tube (ε)	0.92

2. PLAIN SMOOTH ABSORBER TUBE

2.1 Thermal Efficiency Analysis of the Tube

Assumptions: One-dimensional, steady-state conduction with no internal generation

First, energy conservation (Equation 1) to the control surface of Figure 1 is applied:

$$E_{in} - E_{out} + E_g = \frac{dE_{st}}{dt} \quad (1)$$

Since there is no internal generation, and the conduction is steady-state, $E_g = 0$, $\frac{dE_{st}}{dt} = 0$: then

$$E_{in} - E_{out} = 0 \quad (2)$$

If the control surface is the outer surface of absorber tube, then:

$$q_{SolAbs\,-a} - q_{rad\,-a-sky} - q_{conv\,-a-air} - q_{cond\,-sup} = q_{cond\,-a} \quad (3)$$

If the control surface is the inner surface of absorber tube, then:

$$q_{conv\,-fluid} = q_{cond\,-a} \quad (4)$$

To calculate the thermal loss of the absorber tube, the following equation can be used:

$$q_{Thermal\ \ Loss,p} = q_{cond\,-sup} + q_{conv\,-a-air} + q_{rad\,-a-sky} \quad (5)$$

Therefore, the PTSC thermal efficiency with a plain absorber tube could be calculated by the following equation [2]:

$$\eta_{Thermal\ ,p} = \frac{q_{SolAbs} - q_{Thermal\ \ Loss,p}}{GA_a} \quad (6)$$

* Faculty of Engineering, Persian Gulf University, Bushehr, Iran.

[1] Corresponding Author's Tel: +989177754752.
E-mail: xh.jxjamali@yahoo.com

Considering Equations 3, 4, and 5, the higher $q_{conv-fluid}$ is, the higher q_{cond-a} and consequently PTSC thermal efficiency, $\eta_{Thermal,p}$, are.
Also note that $q_{conv-fluid}$ is as follows:

$$q_{conv-fluid} = h_f A(T_s - T_f) \quad (7)$$

It could be understood from the above-mentioned equations that the higher h_f is, the higher PTSC thermal efficiency, $\eta_{Thermal}$, is.

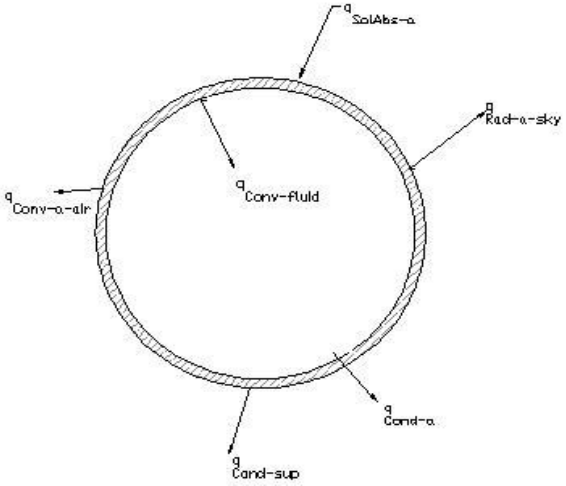

Fig. 1. Control surface of PTSC absorber tube.

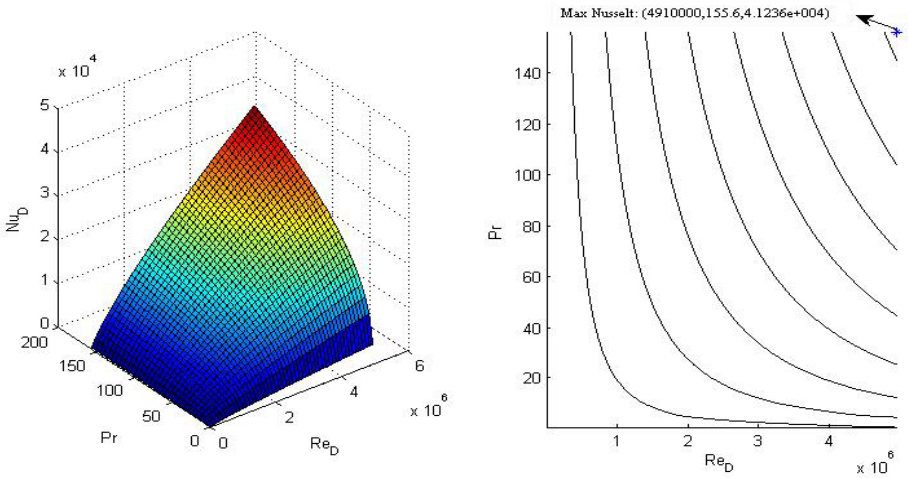

Fig. 2. The oil flow Nusselt number variation with its Prandtl number and Reynolds number; and the contour diagram.

2.1.1 Internal Flow in a Smooth Absorber Tube with Transition and Turbulent Condition

Considering a fully developed turbulent flow in a smooth circular tube, the local Nusselt number may be obtained from Dittus Boelter equation [2]:

$$Nu_D = 0.023\, Re_D^{4/5} Pr^{0.4} \quad (8)$$

As shown in Figure 2 with a 3D diagram and its contour diagram in the xy-plane, the local Nusselt number variation, in a varying range of Prandtl number and Reynolds number for the above-mentioned flow type is shown. The maximum local Nusselt number at special Prandtl and Reynolds numbers is determined on the contour diagram in Figure 2. This maximum point shows the maximum convection coefficient which is its most suitable value for a higher PTSC thermal efficiency according to Equations 3 and 6.

To analyze the effect of fluid viscosity variation on PTSC thermal efficiency using Nusselt number, Sieder and Tate equation [3] is recommended:

$$Nu_D = 0.027\, Re_D^{4/5}\, Pr^{1/3} \left(\frac{\mu}{\mu_s}\right)^{0.14} \quad (9)$$

Where all properties except for μ_s are evaluated at T_m.

Figure 3 shows the maximum Nusselt numbers for the lowest and highest values of Reynolds for the above-mentioned flow type both taking place at the same viscosity and Prandtl number. So, it could be understood that the highest Reynolds number at the mentioned

viscosity and Prandtl number gives the highest Nusselt number or convection coefficient which will lead to a higher PTSC thermal efficiency according to Equations 3 and 6.

To analyze the effect of friction factor on PTSC thermal efficiency, the following correlation including friction factor is presented by Gnielinski [4] for both transition and turbulent regions:

$$Nu_D = \frac{\left(f/8\right)\left(Re_D - 1000\right)Pr}{1 + 12.7\left(f/8\right)^{1/2}\left(Pr^{2/3} - 1\right)} \qquad (10)$$

Where the friction factor may be obtained from Petukhov correlation [5]:

$$f = (0.790 \ln Re_D - 1.64)^{-2} \qquad (11)$$

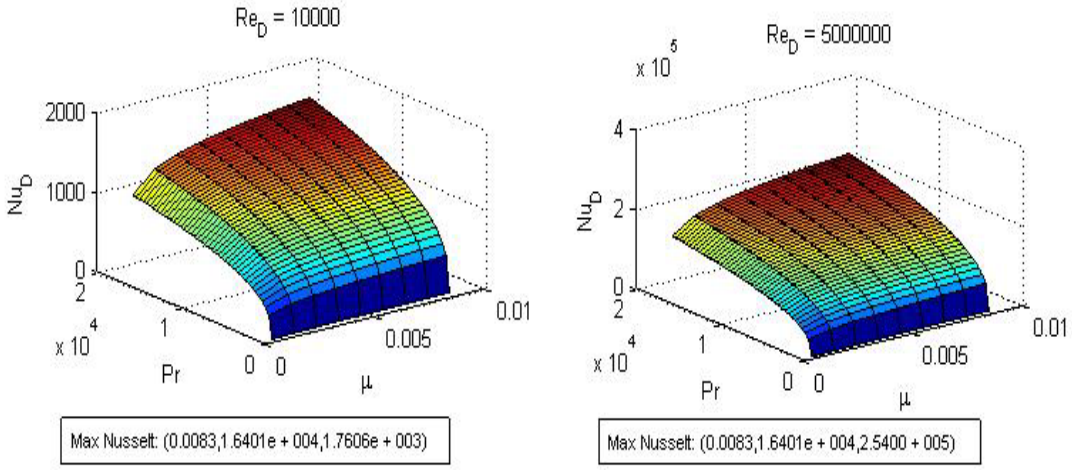

Fig. 3. The oil flow Nusselt number variation with its Prandtl number and viscosity at a) Minimum Reynolds number b) Maximum Reynolds number.

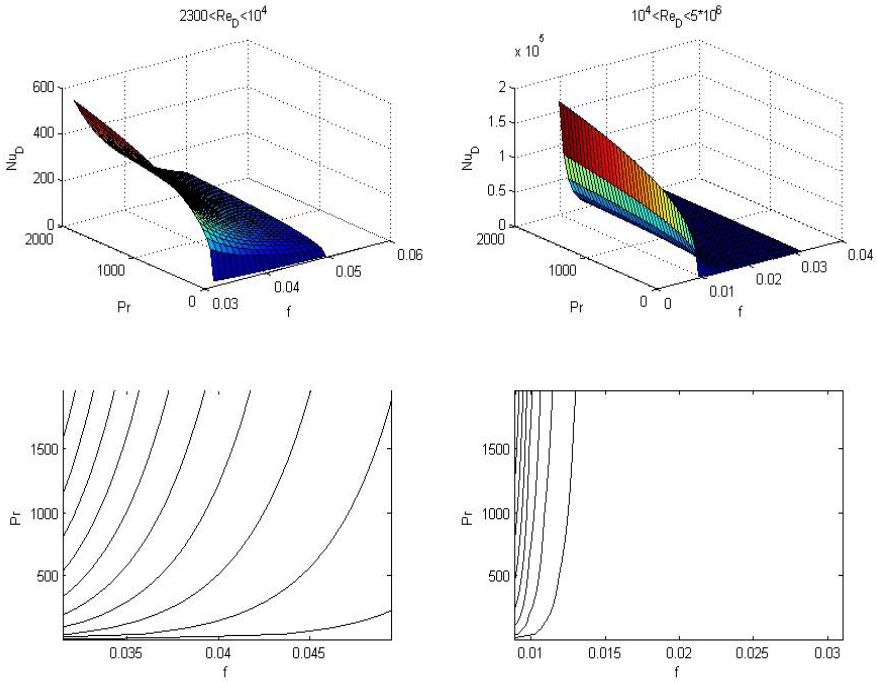

Fig. 4. The oil flow Nusselt number variation with its Prandtl number and friction factor in a) Transition region b) Turbulent region; and the contour diagrams.

As seen in Figures 4a and 4b, the 3D diagrams and their contour diagrams, according to Gnielinski correlation, friction factor on the one hand plays an unfavorable role in increasing Nusselt number, and consequently in promoting PTSC thermal efficiency according to Equations 3 and 6, while this unfavorable effect lessens when Reynolds number changes from transition region to turbulent one; therefore, this considerable rise in Nusselt number in turbulent region will result in PTSC thermal efficiency increase. But on the other hand, when it comes to comparison between an absorber tube with friction and an absorber tube without friction, comparing Figure 2 with Figure 4, it is observed that the maximum Nusselt number considering friction factor effect (Figure 5) is higher than the one resulted with no friction factor consideration (Figure 3), promoting PTSC thermal efficiency. It should also be noted that the Prandtl number increase in both regions,

contrary to the friction factor, will lead to the Nusselt number rise and finally to PTSC thermal efficiency increase.

3. PLAIN ENHANCED ABSORBER TUBE

3.1 Tube Geometries

Rabas (1989) has demonstrated that separation-and-reattachment mechanism ranks high with respect to enhancement quality and energy efficiency, and also it is inferior to only the swirl-induced mechanisms [6]. Internal helical fins or ribs, corrugations and twisted tapes impart a swirl effect on fluid; this effect tends to increase the effective flow length of fluid through the tube, which increases heat transfer and pressure drop [7].

For internal helical fins, ribs and corrugations however, the effect of swirl tends to decrease or disappear all together at higher helix angles since the fluid flow then simply passes axially over the fins or ribs [7]. For twisted tape inserts, the swirl effect on heat transfer augmentation plays an important role [7]. In this section of the paper, mechanisms of turbulent heat transfer augmentation: with surface roughness, with twisted tape inserts, in corrugated tubes, and in internally finned or ribbed tubes will be discussed.

3.1.1 Surface Roughness

The internal roughness of absorber tube is a means to enhance heat transfer coefficient of its internal flow so that PTSC thermal efficiency could then considerably increase. The Churchill (1983) correlation can be used in order to analyze the effect of the friction factor of rough tubes with a commercial pipe roughness of e on convective heat transfer coefficient enhancement [7]:

$$\sqrt{\frac{2}{f}} = -2.46 \ln\left[\frac{e}{d_i} + \left(\frac{7}{Re}\right)^{0.9}\right] \quad (12)$$

Correlation (16) can be used in conjunction with the following expression for predicting the pressure drop in the absorber tube [7]:

$$\Delta p = \frac{2f\dot{m}^2 L}{\rho d_i} \quad (13)$$

The transition flow and fully developed turbulent flow Nusselt number correlation for the internally rough tube could be analyzed by Gnielinski's as reported in Bhatti and Shah's publication (1987) [4]:

$$Nu = \frac{\left(f/2\right)(Re - 1000)Pr}{1 + 12.7\left(f/2\right)^{1/2}\left(Pr^{2/3} - 1\right)} \quad (14)$$

To see the direct influence of the internal roughness, e, of absorber tube on Nusselt number, Figure 5, the 3D diagram and its contour can be used. Considering Equations 12 and 14 at the same time, it can be observed from Figure 5 how the internal roughness of absorber tube and Reynolds number of fluid both favorably influence Nusselt number and finally increase PTSC thermal efficiency, according to Equations 3 and 6. It should be noted that the higher Reynolds number is, the higher gradient of Nusselt number vs. roughness, e, is, as seen from dark blue lines to dark red lines in Figure 5.

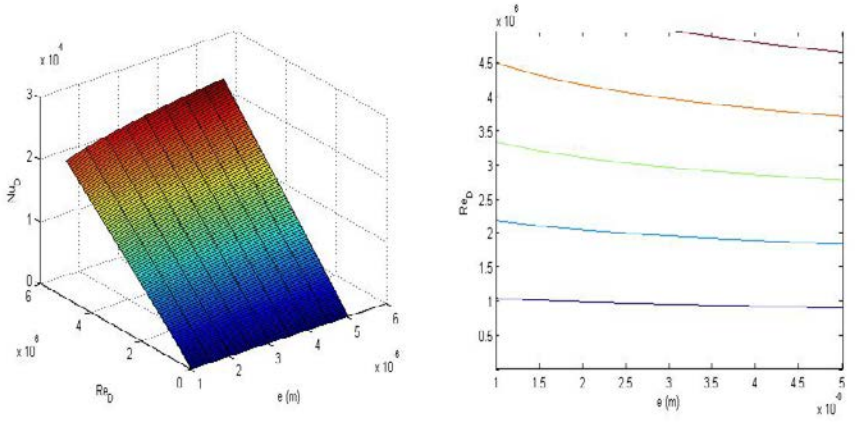

Fig. 5. The oil flow Nusselt number variation with its Reynolds number and internal roughness of absorber tube; and the contour diagram.

3.1.2 Twisted Tape Inserts

Numerous experimental studies have investigated turbulent flow heat transfer with twisted tape inserts inside tube and proposed correlations to predict heat transfer and pressure drop. To analyze the turbulent flow heat transfer inside an absorber tube with twisted tape inserts, Manglik and Bergles (1992) can be referred to. Manglik and Bergles (1992) proposed the following correlation to analyze friction factor within inside a tube with twisted tape inserts [7]:

$$f = \frac{0.0791}{Re^{0.25}}\left[\frac{\pi}{\pi - 4\left(\delta/d_i\right)}\right]^{1.75}\left[\frac{\pi + 2 - 2\left(\delta/d_i\right)}{\pi - 4\left(\delta/d_i\right)}\right]^{1.25}\left[1 + \frac{2.752}{y^{1.29}}\right] \quad (15)$$

Where the value of Re in this expression is based on the flow in the tube without inserts, that is:

$$Re = \frac{\dot{m}d}{\mu} \tag{16}$$

And y is the twist ratio based on the axial length for a 180° turn, δ is the thickness of the tape, and d_i is the internal diameter of the bare tube. The corresponding heat transfer correlation for turbulent flows gives the twisted tape Nusselt number as [7]:

$$\frac{Nu_{tt}}{Nu_{y=\infty}} = 1 + \frac{0.769}{y} \tag{17}$$

Where the Nusselt number for a straight tape without twist ($y = \infty$) is [7]:

$$Nu_{y=\infty} = 0.023\, Re^{0.8} Pr^{0.4} \left[\frac{\pi}{\pi - 4\left(\delta/d_i\right)}\right]^{0.8} \left[\frac{\pi}{\pi - 4\left(\delta/d_i\right)}\right]^{0.2} \emptyset \tag{18}$$

Where $\emptyset$ factor is [7]:

$$\emptyset = \left(\frac{\mu_{bulk}}{\mu_{wall}}\right)^{0.18} \tag{19}$$

Figure 6, the 3D diagram and its contour, clearly depicts how Reynolds number varies more sharply in a higher $\frac{\delta}{d_i}$ ratio. It could also be seen from Figure 6 that friction increases as the gradient of $\frac{\delta}{d_i}$ vs. Re_D increases.

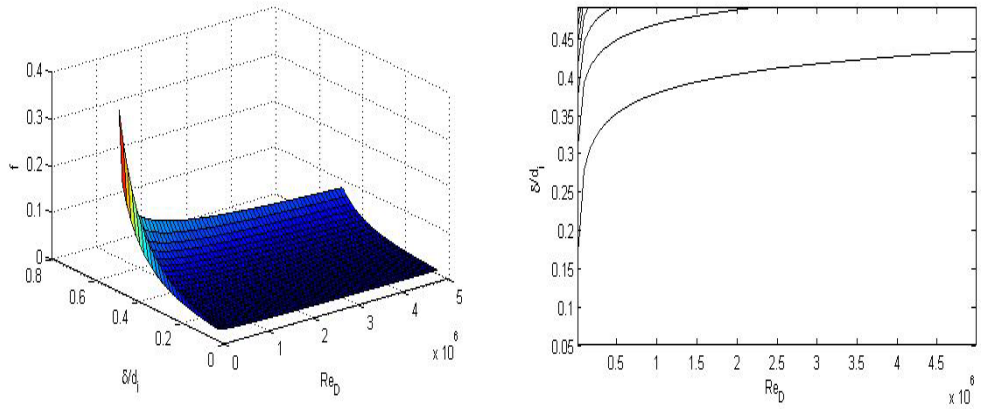

Fig. 6. The influence of $\frac{\delta}{d_i}$ ratio and the oil flow Reynolds number variation on its friction factor; and the contour diagram.

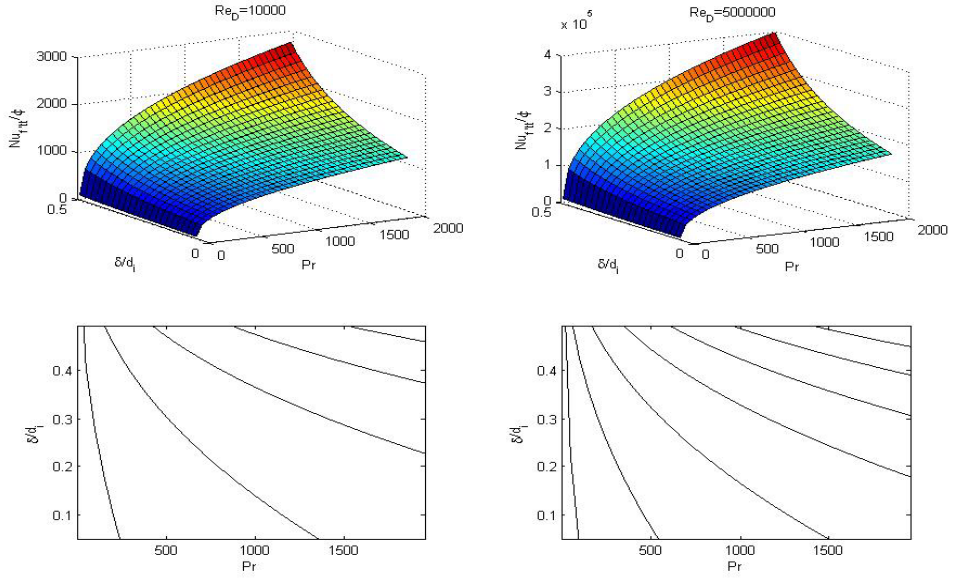

Fig. 7. Variation of the oil flow Nusselt number per ϕ factor with $\frac{\delta}{d_i}$ ratio and its Prandtl number at a) Minimum Reynolds number b) Maximum Reynolds number, in absorber tube with twisted tape inserts; and the contour diagrams.

To see the direct influence of the thickness of the tape on Nusselt number, Figure 7 shows how Nusselt number at one specific Prandtl number increases as $\frac{\delta}{d_i}$ ratio rises. In addition, the higher Prandtl number is, the higher Nusselt number is.

Comparing Figure 7a to Figure 7b, it is observed how $\frac{Nu_{f,tt}}{\emptyset}$ ratio vs. $\frac{\delta}{d_i}$ and Prandtl number varies in the lowest and highest Reynolds number as samples of Reynolds number in turbulent region respectively.

3.1.3 Corrugated Absorber Tubes

Many corrugated tube types have been studied over the years. Withers (1980) presented the following friction factor correlation for Wolverine Kordense tube [7]:

$$\sqrt{\frac{2}{f}} = -2.46 \ln\left[r + \left(\frac{7}{Re}\right)^{m}\right] \quad (20)$$

He also obtained a correlation for the heat transfer coefficient, h_{ct}, in U.S units for Wolverine Kordense tubes [7]:

$$h_c = \frac{c_p \dot{m} \sqrt{f/2}}{\beta_{ct} \Pr\left(Re\sqrt{f/2}\right)^{0.127} + \gamma} \quad (21)$$

Where Re is the plain absorber tube Reynolds number based on the maximum internal diameter of the corrugated tube, d_i, and $\dot{m}$ is mass flux or velocity in $lb/h\,ft^2$. The value of his empirical constant β_{ct} is specific to each tube size and type. It varies in value from about 5.0 to 7.2; its medium value for all types is 6.0 [7]. The actual values for these parameters can be found in the appropriate Wolverine Engineering Databook II table on Kordense tube of MHT type. The values of the design constants are $m = 0.44$, $r = 0.00595$, $\gamma = 2.56$ [7]. Having the friction factor, the pressure drop for a corrugated tube of length L can be calculated using Equation 13. As shown in Figure 8, friction factor sharply dwindles in low Reynolds numbers of turbulent region while the decrease in middle Reynolds numbers of turbulent region is mild, insofar as friction factor becomes almost constant in high Reynolds numbers of the region.

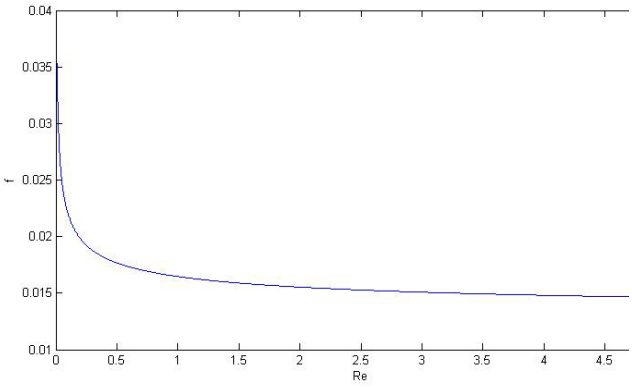

Fig. 8. Reynolds number influence on the oil flow friction factor in corrugated absorber tube.

As depicted in Figure 9, the 3D diagram and its contour, friction factor rises more sharply in low Reynolds numbers (the yellow lines to dark red lines shown in Figure 9) and vice versa in high Reynolds numbers (the dark blue lines to green lines shown in Figure 9). Therefore, according to Figures 8 and 9, a higher convection coefficient can be obtained at a higher friction factor and a lower Reynolds number.

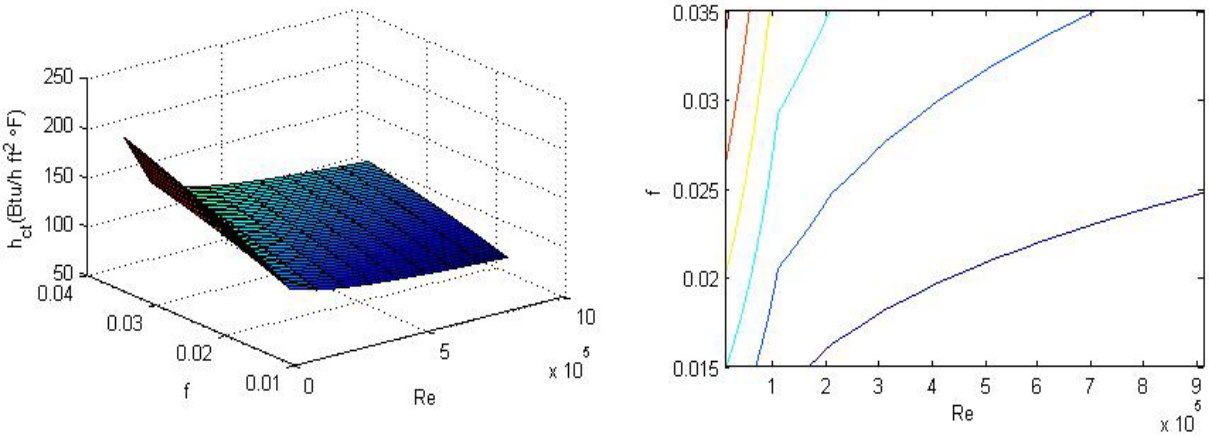

Fig. 9. Variation of the oil convective heat transfer coefficient with its friction factor and Reynolds number in corrugated absorber tube; and the contour diagram.

3.1.4 Internally Finned or Ribbed Absorber Tube

Ravigurujan and Bergles (1985) have proposed the most general and accurate method which is reliable for predicting heat transfer and pressure drop inside internally ribbed tubes (and plain tubes with coiled wire inserts) and also most internally finned tubes [7]. The rib geometries and profiles (and wire geometry) that they included in their study are depicted in Figures 10 to 12, where e is the height of the rib or diameter of the wire, p is the axial pitch from one rib (or wire) to the next, β is the helix angle of the rib or wire relative to the tube axis, β_{rib} is the profile contact angle of the rib to the internal surface of the tube, and $n_{corners}$ is the number of sharp corners of the rib facing the flow (two for triangle or rectangular cross-section ribs and infinity for smoother profiles) [7]. Figures 10 to 12 reveal how friction factor varies with Reynolds number and the axial pitch, p, for equilateral triangle profile, rectangular profile, and circular profile respectively. It should be mentioned that

the profile contact angle for a circular profile is taken as 90° [7]. This method is applicable to the following range of parameters: $0.1 < {}^{e}/_{d_i} < 0.2$, $0.1 < {}^{p}/_{d_i} < 7.0$, $0.3 < {}^{\beta}/_{90} < 1.0$, $5000 < Re < 250000$, and $0.66 < Pr < 37.6$ [7]. The ribbed tube friction factor is correlated as a ratio to the value for a smooth tube of the same internal diameter as [7]:

$$\frac{f_{ft}}{f} = \left\{ 1 + \left[29.1 Re^{\left(0.67-0.06\,{}^{p}/_{d_i}-0.49\,{}^{\beta}/_{90}\right)} \left(\frac{e}{d_i}\right)^{\left(1.37-0.157\,{}^{p}/_{d_i}\right)} \cdot \left(\frac{p}{d_i}\right)^{\left(-0.00000166\,Re-0.33\,{}^{\beta}/_{90}\right)} \cdot \left(\frac{\beta}{90}\right)^{\left(4.59+0.00000411\,Re-0.15\,{}^{p}/_{d_i}\right)} \cdot \left(1 + \frac{2.94}{n_{corners}}\right) \sin\beta_{rib} \right]^{{}^{15}/_{16}} \right\}^{{}^{16}/_{15}} \quad (22)$$

Where f is the friction factor of the reference tube (plain tube with smooth internal surface) which could be determined using Equation 23, applying the wall-to-bulk property ratios [7]. The pressure drop is then obtained, applying Equation 13 and using the ribbed tube friction factor in place of the plain tube value and also using the diameter of the ribs, d_i [7].

$$f = (1.58 \ln Re - 3.28)^{-2} \quad (23)$$

Figures 10 to 12, the 3D diagrams and their contours for three different randomly chosen e values, show how friction factor varies with both axial pitch and Reynolds number for triangle profile, rectangular profile, and circular profile respectively. As shown in Figures 10 to 12, the presence of red lines (the highest friction factors) in low to middle Reynolds numbers (of the firstly determined range of Reynolds number for Equation 22) for higher e values is more obvious than that for lower e values; in other words, the highest values of friction factor in lower values of e take place at lower values of axial pitch so as to compensate for the unfavorable effect of lower e. In addition, the gradient of axial pitch vs. Reynolds number in low friction factors is negative; while the gradient, in high friction factors, is positive in low Reynolds number and negative in high Reynolds number, as shown in Figures 10 to 12. It should also be noted that the absolute value of the above-mentioned gradient decreases at high friction factors.

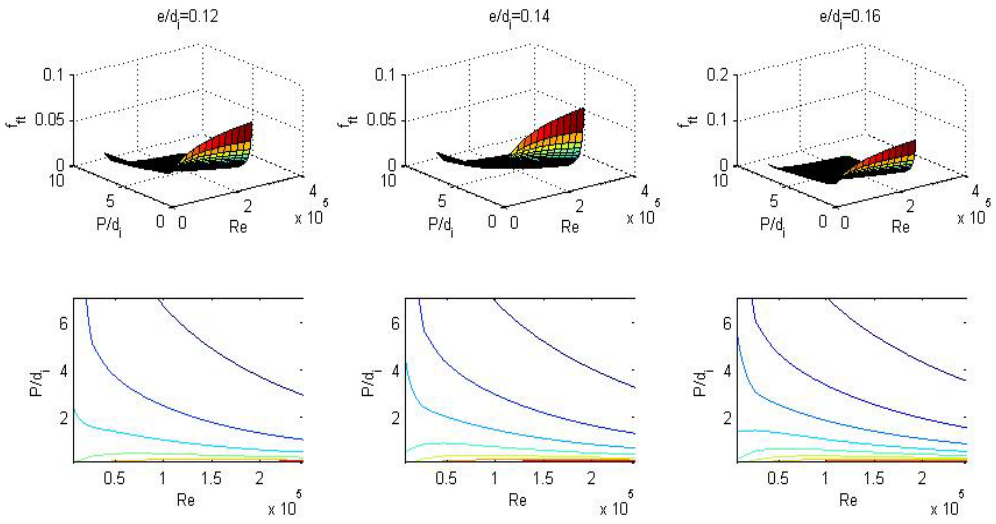

Fig. 10. The influence of $\frac{P}{d_i}$ ratio and the oil flow Reynolds number on its friction factor in internally finned or ribbed tube with *triangle* profile at a)$\frac{e}{d_i} = 0.12$ b)$\frac{e}{d_i} = 0.14$ c)$\frac{e}{d_i} = 0.16$; and the contour diagrams.

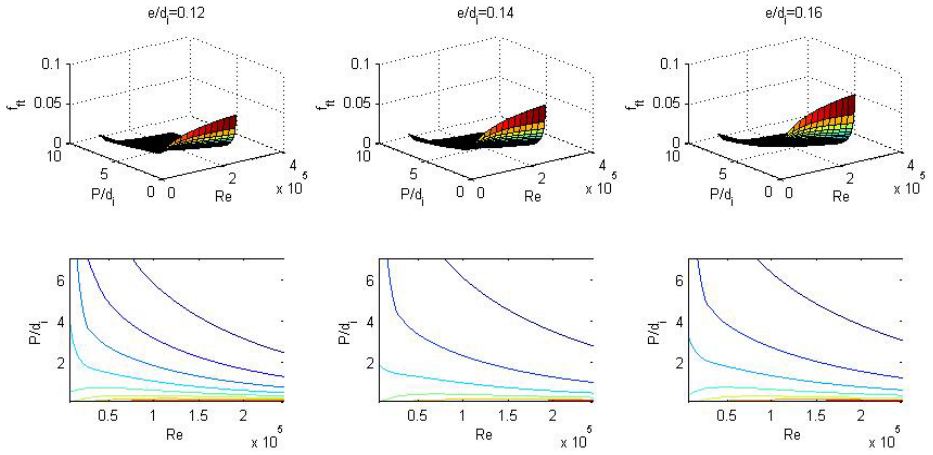

Fig. 11. The influence of $\frac{p}{d_i}$ ratio and the oil flow Reynolds number on its friction factor in internally finned or ribbed tube with *rectangular* profile at *a*) $\frac{e}{d_i} = 0.12$ b) $\frac{e}{d_i} = 0.14$ c) $\frac{e}{d_i} = 0.16$; and the contour diagrams.

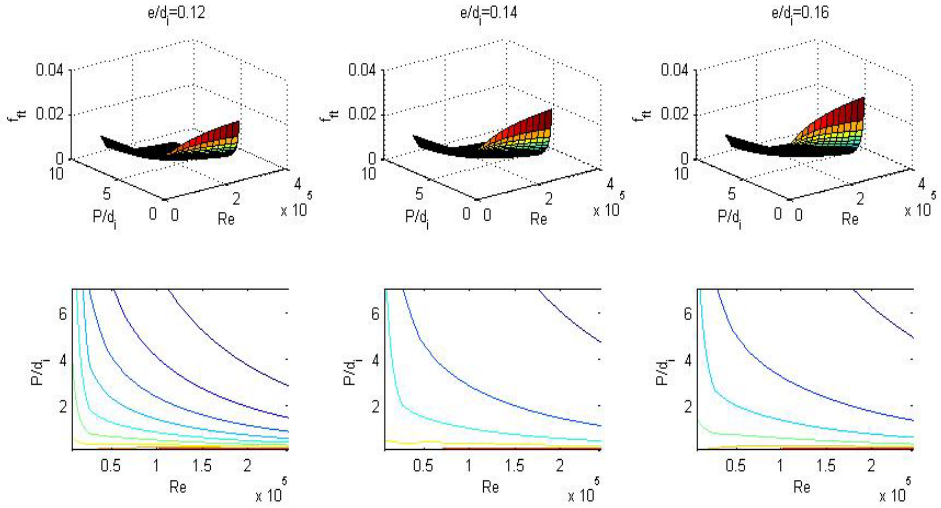

Fig. 11. The influence of $\frac{p}{d_i}$ ratio and the oil flow Reynolds number on its friction factor in internally finned or ribbed tube with *circular* profile at *a*) $\frac{e}{d_i} = 0.12$ b) $\frac{e}{d_i} = 0.14$ c) $\frac{e}{d_i} = 0.16$; and the contour diagrams.

Comparing Figures 10 to 12 to each other, it could be concluded that the triangle profile (Figure 10) and the circular profile (Figure 12) yield the highest and the lowest friction factors respectively. This comparison also shows that the gradient of axial pitch vs. Reynolds number for the circular profile and the triangle profile at low Reynolds numbers varies respectively the least and the most with Reynolds number variation; this fact could specially be sensed at lower e values.

The ribbed tube heat transfer can also be calculated using the following correlation [7]:

$$\frac{h_{ft}}{h_{pt}} = \left\{1 + \left[2.64Re^{0.036}\left(\frac{e}{d_i}\right)^{0.212}\left(\frac{p}{d_i}\right)^{-0.21}\left(\frac{\beta}{90}\right)^{0.29}Pr^{-0.024}\right]^7\right\}^{1/7} \quad (24)$$

where h_{pt} could be determined using Equation 25 [7]:

$$Nu = \frac{h_{pt}\,d_i}{k} = \frac{\left(f/2\right)(Re-1000)Pr}{1+12.7\left(f/2\right)^{1/2}\left(Pr^{2/3}-1\right)}\left(\frac{\mu_{bulk}}{\mu_{wall}}\right)^{0.14} \quad (25)$$

where the friction factor of the reference tube (plain tube with smooth internal surface) could be determined with Equation 23 [7]. Considering $\emptyset = \left(\frac{\mu_{bulk}}{\mu_{wall}}\right)^{0.14}$, Figure 5 can be used to analyze $\frac{Nu}{\emptyset}$ variation as a function in Equation 25. As mentioned before, the value of Nusselt number with friction factor effect is higher than the one without friction factor effect. Therefore, the higher value of f is, the higher value of h_{pt} and consequently h_{ft} are based on Equation 24.

4. ABSORBER TUBE WITH VACUUM GLASS TUBE

As mentioned in Equation 5, $q_{Conv-a-air}$ is one factor in PTSC thermal loss. Therefore, applying a vacuum glass cover to the plain absorber tube in order to minimize the effect of this unfavorable factor in the wake of minimizing the convective heat transfer between the absorber and the air around it will result in a considerable increase in PTSC thermal efficiency comparing Equations 5 and 28. The following analysis is made to obtain the PTSC thermal efficiency for an absorber tube with vacuum glass tube.

If the control surface in Figure 13 is the outer surface of glass tube, then:

$$E_{in} - E_{out} = q_{cond} \quad (26)$$

$$q_{conv-g-air} + q_{rad-g-sky} - q_{SolAbs-g} = q_{cond-g} \quad (27)$$

$$q_{ThermalLoss,g} = q_{rad-g-sky} + q_{conv-g-air} + q_{cond-sup} \quad (28)$$

If the control surface in Figure 13 is the inner surface of glass tube, regarding Equation 26, then:

$$q_{conv-a-g} + q_{rad-a-g} = q_{cond-g} \quad (29)$$

If the control surface in Figure 13 is the outer surface of the absorber tube, regarding Equation 26, then:

$$q_{SolAbs-a} - q_{conv-a-g} - q_{rad-a-g} - q_{cond-sup} = q_{cond-a} \quad (30)$$

If the control surface in Figure 13 is the inner surface of the absorber tube, regarding Equation 26, then:

$$q_{conv-fluid} = q_{cond-a} \quad (31)$$

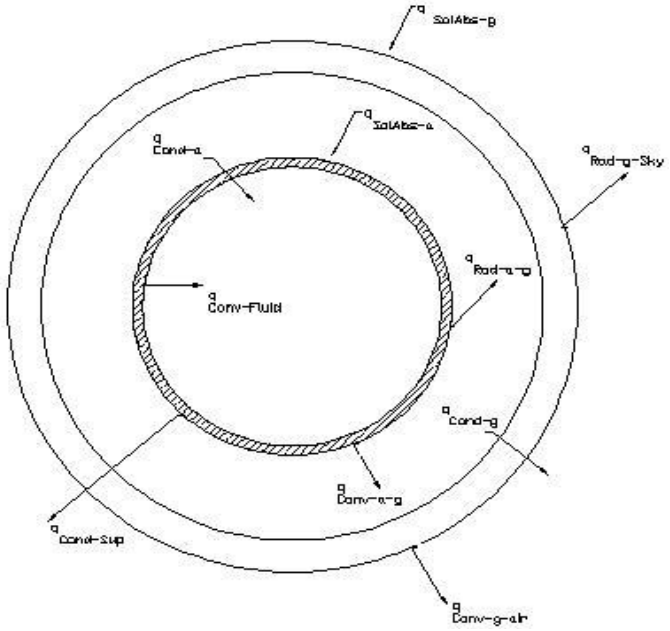

Fig. 13. Control surface of PTSC absorber tube with glass cover.

It should be noted that, in case of using glass tube, convective heat transfer between absorber tube and glass tube is considered 0 $^{W}/_{m^2}$. In addition, in all calculations in the paper, conductive heat transfer from outer surface of absorber tube to support structure is assumed to be negligible.

Therefore, the PTSC thermal efficiency for an absorber tube with vacuum glass tube could be calculated by the following equation [8]:

$$\eta_{Thermal,g} = \frac{q_{SolAbs} - q_{ThermalLoss,g}}{AG_s} \quad (32)$$

Where according to Equations 28, 30 and 31 and mentioned assumptions:

$$q_{SolAbs} - q_{ThermalLoss,g} = q_{rad-a-g} + q_{conv-fluid} - q_{rad-g-sky} - q_{conv-g-air} \quad (33)$$

5. EXTERNAL FLOW OVER SMOOTH ABSORBER TUBE WITH GLASS TUBE

Regarding Equation 28, $q_{Conv-g-air}$ is an influential factor in thermal loss of PTSC with glass tube, which shows the important role of air flow over PTSC glass and the convective heat transfer coefficient of the air, h_a, in result. in particular for power plants like Shiraz solar power plant located in the windy area [9]. Considering a windy air flow over the PTSC, an expression given by Mullick and Nanda can be employed to calculate the convective heat transfer coefficient of the ambient air [10]:

$$h_a = 4d^{0.42}v^{0.5} \quad (34)$$

Where v is wind velocity in $^{m}/_{s}$ and d is the outer diameter of glass cover in m.

Therefore, Nusselt number can be obtained by the following equation:

$$Nu = \frac{h_a d}{k} = \frac{4d^{1.42}v^{0.5}}{k} \quad (35)$$

Calculating h_a using Equation 34, $q_{conv-g-air}$ could be obtained for an absorber tube with vacuum glass envelope as follows:

$$q_{conv-g-air} = h_a(T_g - T_a) \quad (36)$$

Having h_a from the calculations, $q_{conv-a-air}$ for an absorber tube without a glass envelope can be obtained as follows:

$$q_{conv-a-air} = h_a(T_{s,a} - T_a) \quad (37)$$

Since the absorber surface temperature, $T_{s,a}$, is considerably higher than the glass surface temperature, T_g, it can be easily understood from Equations 36 and 37 in the above-mentioned analysis that $q_{Conv-a-air}$ is considerably higher than $q_{Conv-g-air}$. Therefore, the thermal loss of the PTSC with glass tube will be noticeably lower than it without glass tube according to Equations 5 and 28, which will result in the higher thermal efficiency of the PTSC with glass tube.

6. CONCLUSION

Comparing the plain smooth absorber tube with the plain enhanced absorber tube according to the numerical results obtained (Tables 2 and 3) using the mentioned formulas and the diagrams relevant to them, it is understood that the convective heat transfer coefficient of PTSC internal flow, h_f, and finally its thermal efficiency can be increased by using the internal enhancements for the absorber tube, as the swirl-induced mechanisms were discussed in this article. In addition, considering the unfavorable effect of the convective heat transfer coefficient of the air, h_a, on PTSC thermal efficiency, and also the formulas and the diagrams rendered on this issue, it is concluded how by using a glass cover, this unfavorable effect would lessen or completely disappear, and the thermal efficiency of plain enhanced absorber tube- which was itself higher than that of plain smooth absorber tube- would remarkably increase (as shown in Tables 2, 3, 4, and 5). Table 5 shows how the second and third modes of PTSC are integrated together in order to improve the first mode of PTSC. In Table 6, a comparison of thermal efficiencies of PTSC with enhanced absorber tube equipped with glass tube and one without glass tube is made. This comparison clearly shows how, at the given Reynolds and Prandtl numbers, PTSC thermal efficiency can be raised by applying vacuum glass tube and different enhancements together to the plain smooth absorber tube.

Table 2. Efficiency calculations of PTSC with plain smooth absorber tube.

Reynolds number (*Re*)	79300
Prandtl number (*Pr*)	7.25
Fluid temperature (T_f)	100 ˚ *C*
Thermal conductivity of oil (k), [11]	0.127 *W/m˚C*
Difference between absorber tube surface temperature ($T_{s,a}$) and fluid temperature (T_f)	0.25 ˚ *C*
Nusselt number ($Nu = 0.012(Re^{0.87} - 280)Pr^{0.4}$), [12]	483
Convective heat transfer coefficient ($h_{pt} = \frac{Nu \times k}{D_i}$)	935 W/m^2K
Heat from inner surface of absorber tube to fluid ($q_{conv-fluid}$)	233.75 W/m^2
Sun angle	28.92
Solar irradiation (G)	836 W/m^2
PTSC thermal efficiency ($\eta_{Thermal,p}$)	0.28

Table 3a. Efficiency calculations of PTSC with plain enhanced absorber tube (twisted tape inserts).

Reynolds number (*Re*)	79300
Prandtl number (*Pr*)	7.25
Fluid temperature (T_f)	100 ˚*C*
Thermal conductivity of oil (k), [11]	0.127 $W/m˚C$
Difference between absorber tube surface temperature ($T_{s,a}$) and fluid temperature (T_f)	0.25 ˚ *C*
$\frac{\delta}{d_i}$ ratio	0.06
ϕ factor	1
Nusselt number (*Nu*)	654.57
Convective heat transfer coefficient (h_{tt})	1267.23 W/m^2K
Heat from inner surface of absorber tube to fluid ($q_{conv-fluid}$)	316.8 W/m^2
Sun angle	28.92
Solar irradiation (G)	836 W/m^2
PTSC thermal efficiency ($\eta_{Thermal,p,tt}$)	0.37

Table 3b. Efficiency calculations of PTSC with plain enhanced absorber tube (corrugated tube).

Reynolds number (*Re*)	79300
Prandtl number (*Pr*)	7.25
Fluid temperature (T_f)	100 ˚C
Thermal conductivity of oil (k), [11]	0.127 $^{W}/_{m^{\circ}C}$
Difference between absorber tube surface temperature ($T_{s,a}$) and fluid temperature (T_f)	0.25 ˚ C
Heat capacity (C_p),[11]	1.773 $^{kj}/_{kg\,^{\circ}C}$
Friction factor	0.0229
Mass rate ($\dot{m}$)	1.56 $^{kg}/_{s}$
Convective heat transfer coefficient (h_{ct})	626.4 $^{W}/_{m^2K}$
Heat from inner surface of absorber tube to fluid ($q_{conv-fluid}$)	157.35 $^{W}/_{m^2}$
Sun angle	28.92
Solar irradiation (G)	836 $^{W}/_{m^2}$
PTSC thermal efficiency ($\eta_{Thermal,p,ct}$)	0.18

Table 3c. Efficiency calculations of PTSC with plain enhanced absorber tube (internally finned or ribbed tube).

Reynolds number (*Re*)	79300
Prandtl number (*Pr*)	7.25
Fluid temperature (T_f)	100 ˚C
Thermal conductivity of oil (k), [11]	0.127 $^{W}/_{m\,^{\circ}C}$
Difference between absorber tube surface temperature ($T_{s,a}$) and fluid temperature (T_f)	0.25 ˚ C
Friction factor (f_{ft})	0.0139
$^{p}/_{d_i}$ ratio	6
$^{e}/_{d_i}$ ratio	0.16
Profile contact angle (β_{rib})	60˚ for equilateral triangle profile
Helix angle (β)	30˚
ϕ factor	1
Convective heat transfer coefficient (h_{ft})	1957.95 $^{W}/_{m^2K}$
Heat from inner surface of absorber tube to fluid ($q_{conv-fluid}$)	233.75 $^{W}/_{m^2}$
Sun angle	28.92
Solar irradiation (G)	836 $^{W}/_{m^2}$
PTSC thermal efficiency ($\eta_{Thermal,p,ft}$)	0.58

Table 4. Efficiency calculations of PTSC with non-enhanced absorber tube equipped with glass cover.

Reynolds number (*Re*)	79300
Prandtl number (*Pr*)	7.25
Fluid temperature (T_f)	215.85 ˚C
Thermal conductivity of oil (k), [11]	0.111 $^{W}/_{m\,^{\circ}C}$
Absorber tube surface temperature ($T_{s,a}$)	216.1 ˚C
Difference between absorber tube surface temperature ($T_{s,a}$) and fluid temperature (T_f)	0.25 ˚ C
Glass cover surface temperature (T_g)	47 ˚C
Ambient temperature (T_a)	33 ˚C
Effective sky temperature (T_{sky})	20 ˚C
Nusselt number (Nu=0.012($Re^{0.87}-280$)$Pr^{0.4}$), [12]	475.63
Convective heat transfer coefficient ($h_{gc}=\frac{Nu\times k}{D_i}$)	804.8 $^{W}/_{m^2K}$
Heat from inner surface of absorber tube to working fluid by convection ($q_{conv-fluid}$)	201.2 $^{W}/_{m^2}$
Heat from outer surface of absorber tube to inner surface of glass cover by radiation ($q_{rad-a-g}$=εσ($T_{s,a}^4-T_g^4$))	397.52 $^{W}/_{m^2}$
Heat from glass cover to sky by radiation ($q_{rad-g-sky}$=εσ($T_{g,s}^4-T_{sky}^4$))	162.52 $^{W}/_{m^2}$
Heat from glass cover to ambient air by convection ($q_{conv-g-air}$)	28.63 $^{W}/_{m^2}$

Heat from outer surface of absorber tube to inner surface of glass cover by convection ($q_{conv-a-g}$)	0 W/m^2
$q_{SolAbs} - q_{ThermalLoss}$, [Refer to Equation 33]	407.57 W/m^2
Sun angle	28.92
Solar irradiation (G)	836 W/m^2
PTSC thermal efficiency ($\eta_{Thermal,g}$)	0.49

Table 5a. Efficiency calculations of PTSC with enhanced absorber tube (twisted tape inserts) equipped with glass cover.

Reynolds number (*Re*)	79300
Prandtl number (*Pr*)	7.25
Fluid temperature (T_f)	215.85 ˚C
Thermal conductivity of oil (k), [11]	0.111 $W/m\,^{\circ}C$
Absorber tube surface temperature ($T_{s,a}$)	216.1 ˚C
Difference between absorber tube surface temperature ($T_{s,a}$) and fluid temperature (T_f)	0.25 ˚C
Glass cover surface temperature (T_g)	47 ˚C
Ambient temperature (T_a)	33 ˚C
Effective sky temperature (T_{sky})	20 ˚C
Nusselt number (Nu)	654.57
Convective heat transfer coefficient ($h_{g,tt} = \frac{Nu \times k}{D_i}$)	1107.58 W/m^2K
Heat from inner surface of absorber tube to working fluid by convection ($q_{conv-fluid}$)	276.895 W/m^2
Heat from outer surface of absorber tube to inner surface of glass cover by radiation ($q_{rad-a-g}$=εσ($T_{s,a}^4 - T_g^4$))	397.52 W/m^2
Heat from glass cover to sky by radiation ($q_{rad-g-sky}$=εσ($T_{g,s}^4 - T_{sky}^4$))	162.52 W/m^2
Heat from glass cover to ambient air by convection ($q_{conv-g-air}$)	28.63 W/m^2
Heat from outer surface of absorber tube to inner surface of glass cover by convection ($q_{conv-a-g}$)	0 W/m^2
$q_{SolAbs} - q_{ThermalLoss}$, [refer to Equation 33]	483.265 W/m^2
Sun angle	28.92
Solar irradiation (G)	836 W/m^2
PTSC thermal efficiency ($\eta_{Thermal,g}$)	0.58

Table 5b. Efficiency calculations of PTSC with enhanced absorber tube (corrugated tube) equipped with glass cover.

Reynolds number (*Re*)	79300
Prandtl number (*Pr*)	7.25
Fluid temperature (T_f)	215.85 ˚C
Thermal conductivity of oil (k), [11]	0.111 $W/m\,^{\circ}C$
Absorber tube surface temperature ($T_{s,a}$)	216.1 ˚C
Difference between absorber tube surface temperature ($T_{s,a}$) and fluid temperature (T_f)	0.25 ˚C
Glass cover surface temperature (T_g)	47 ˚C
Ambient temperature (T_a)	33 ˚C
Effective sky temperature (T_{sky})	20 ˚C
Nusselt number (Nu)	654.57
Convective heat transfer coefficient ($h_{g,ct} = \frac{Nu \times k}{D_i}$)	738.98 W/m^2K
Heat from inner surface of absorber tube to working fluid by convection ($q_{conv-fluid}$)	184.75 W/m^2
Heat from outer surface of absorber tube to inner surface of glass cover by radiation ($q_{rad-a-g}$=εσ($T_{s,a}^4 - T_g^4$))	397.52 W/m^2
Heat from glass cover to sky by radiation ($q_{rad-g-sky}$=εσ($T_{g,s}^4 - T_{sky}^4$))	162.52 W/m^2
Heat from glass cover to ambient air by convection ($q_{conv-g-air}$)	28.63 W/m^2
Heat from outer surface of absorber tube to inner surface of glass cover by convection ($q_{conv-a-g}$)	0 W/m^2

$q_{SolAbs} - q_{ThermalLoss}$, [refer to Equation 33]	391.12 $^{W}/_{m^2}$
Sun angle	28.92
Solar irradiation (G)	836 $^{W}/_{m^2}$
PTSC thermal efficiency ($\eta_{Thermal\ ,g}$)	0.46

Table 5c. Efficiency calculations of PTSC with enhanced absorber tube (internally finned or ribbed tube) equipped with glass cover.

Reynolds number (*Re*)	79300
Prandtl number (*Pr*)	7.25
Fluid temperature (T_f)	215.85 ˚*C*
Thermal conductivity of oil (k), [11]	0.111 $^{W}/_{m^{\circ}C}$
Absorber tube surface temperature ($T_{s,a}$)	216.1 ˚*C*
Difference between absorber tube surface temperature ($T_{s,a}$) and fluid temperature (T_f)	0.25 ˚*C*
Glass cover surface temperature (T_g)	47 ˚*C*
Ambient temperature (T_a)	33 ˚*C*
Effective sky temperature (T_{sky})	20 ˚*C*
Nusselt number (Nu)	654.57
Convective heat transfer coefficient ($h_{g,ft} = \frac{Nu \times k}{D_i}$)	1943.06 $^{W}/_{m^2K}$
Heat from inner surface of absorber tube to working fluid by convection ($q_{conv-fluid}$)	485.76 $^{W}/_{m^2}$
Heat from outer surface of absorber tube to inner surface of glass cover by radiation ($q_{rad-a-g}$=εσ($T_{s,a}^4 - T_g^4$))	397.52 $^{W}/_{m^2}$
Heat from glass cover to sky by radiation ($q_{rad-g-sky}$=εσ($T_{g,s}^4 - T_{sky}^4$))	162.52 $^{W}/_{m^2}$
Heat from glass cover to ambient air by convection ($q_{conv-g-air}$)	28.63 $^{W}/_{m^2}$
Heat from outer surface of absorber tube to inner surface of glass cover by convection ($q_{conv-a-g}$)	0 $^{W}/_{m^2}$
$q_{SolAbs} - q_{ThermalLoss}$, [refer to Equation 33]	495.81 $^{W}/_{m^2}$
Sun angle	28.92
Solar irradiation (G)	836 $^{W}/_{m^2}$
PTSC thermal efficiency ($\eta_{Thermal\ ,g}$)	0.59

Table 6. Comparison of thermal efficiencies of PTSC with enhanced absorber tube equipped with glass cover and one without glass cover.

	Twisted tape inserts	Corrugated tube	Internally finned or ribbed tube
PTSC thermal efficiency with enhanced absorber tube without vacuum glass cover	0.37	0.18	0.58
PTSC thermal efficiency with enhanced absorber tube equipped with vacuum glass cover	0.58	0.46	0.59

ACKNOWLEDGEMENT

I express my special thanks to Dr. H. Eskandari, Assistant Professor of Mechanical Engineering Department, Persian Gulf University, for his encouraging guidelines towards researches in solar energy as clean energy.

NOMENCLATURE

A_a: Collector aperture area (m^2)
D_i: Absorber tube inner diameter (mm)
D_o: Absorber tube outer diameter (mm)
E_{st}: Stored thermal and mechanical energy rate (W)
E_g: Thermal and mechanical energy generation rate (W)
E_{in}: Inflow of thermal and mechanical energy rate (W)
E_{out}: Outflow of thermal and mechanical energy rate (W)
f: Friction factor
f_{ft}: Ribbed tube friction factor
G: Solar irradiance $\left(^{W}/_{m^2}\right)$
h_f: Convective heat transfer coefficient of fluid ($^{W}/_{m^2K}$)
h_{ct}: Convective heat transfer coefficient of fluid for corrugated absorber tube ($^{W}/_{m^2K}$)
h_{ft}: Convective heat transfer coefficient of fluid for internally finned or ribbed absorber tube ($^{W}/_{m^2K}$)
h_{tt}: Convective heat transfer coefficient of fluid for absorber tube with twisted tape inserts ($^{W}/_{m^2K}$)

h_{pt}: Convective heat transfer coefficient of fluid for plain absorber tube ($^{W}/_{m^2K}$)
h_a: Convective heat transfer coefficient of ambient air ($^{W}/_{m^2K}$)
h_g: Convective heat transfer coefficient of fluid for non-enhanced absorber tube with vacuum glass cover ($^{W}/_{m^2K}$)
$h_{g,tt}$: Convective heat transfer coefficient of fluid for enhanced absorber tube (twisted tape inserts) with vacuum glass cover ($^{W}/_{m^2K}$)
$h_{g,ct}$: Convective heat transfer coefficient of fluid for enhanced absorber tube (corrugated tube) with vacuum glass cover ($^{W}/_{m^2K}$)
$h_{g,ft}$: Convective heat transfer coefficient of fluid for enhanced absorber tube (finned tube) with vacuum glass cover ($^{W}/_{m^2K}$)
k: Thermal conductivity ($^{W}/_{m\,K}$)
L: Absorber tube length (m)
m: Design constants
$\dot{m}$: Mass rate ($^{kg}/_{s}$)
Nu: Nusselt Number $\left(Nu = \frac{h \times D}{k_f}\right)$
$Nu_{D,C}$: Corrected Nusselt Number
$Nu_{f,tt}$: Fluid Nusselt Number for absorber tube with twisted tape inserts
Pr: Prandtl Number $\left(Pr = \frac{\mu \times C_p}{k_f}\right)$
ΔP: Pressure drop (Pa)
p: Axial pitch of internally finned or ribbed absorber tube (mm)
$q_{SolAbs\,-a}$: Heat from sunlight to absorber tube (W)
$q_{rad\,-a-sky}$: Heat from absorber tube to sky by radiation (W)
$q_{conv\,-a-air}$: Heat from absorber tube to ambient air by convection (W)
$q_{cond\,-sup}$: Heat from outer surface of absorber tube to support structure by conduction (W)
$q_{cond\,-a}$: Heat from outer surface of absorber tube to inner surface of absorber tube by conduction (W)
$q_{conv\,-fluid}$: Heat from inner surface of absorber tube to working fluid by convection (W)
$q_{Thermal\ \ Loss,p}$: Thermal Loss of plain absorber tube (W)
q_{SolAbs}: Heat gain from sunlight (W)
$q_{conv\,-g-air}$: Heat from glass cover to ambient air by convection (W)
$q_{rad\,-g-sky}$: Heat from glass cover to sky by radiation (W)
$q_{SolAbs\,-g}$: Heat from sunlight to glass cover (W)

REFERENCES

[1] Yaghoubi M., Ahmadi F. and Bandehee M. 2013. Analysis of heat losses of absorber tubes of parabolic trough collector of Shiraz (Iran) solar power plant. *Journal of Clean Energy Technologies*, Vol. 1.

[2] Winterton R.H.S. 1998. Where did the Dittus and Boelter equation come from? *International Journal of Heat Mass Transfer* 41: *809*.

[3] Sieder E.N. and G.E. Tate. 1936. Heat transfer and pressure drop in liquids in tubes. *Ind. Eng. Chem*., 28: 1429-1435.

[4] Ming Qu, Archer D.H. and Masson S.V., 2006. A linear parabolic trough solar collector performance model. In the *Sixth International Conference for Enhanced Building Operations*, Shenzhen, China, 6-9 November. Included in *Renewanle Energy Resources and a Grener Future, Vol. VIII-3-3.*

[5] Petukhov B.S. 1970. *Advances in Heat Transfer*. J.P. Hartnett and T.F. Irvine Jr. (Eds.), Vol. 6. Academic Press, New York.

[6] Mullick S.C. and S.K. Nanda. 1989. An improved technique computing the heat loss factor of a tubular absorber. *Journal of Solar Energy* (42): 1-7.

[7] Gnielinski V., 1976. New equations for heat and mass transfer in turbulent pipe and channel flow. *Int. Chem. Eng.* 16: 359-368.

[8] Bell K.J. and A.C. Mueller. 2001. Enhanced single-phase turbulent tube-side flows and heat transfer. *Wolverine Engineering Data Book*, Vol. II, pp. 3, 4, 13, 18, 19, 20, 24, 26.

[9] Arman B. and T.J. Rabas. 1992. Influence of Prandtl number and effects of disrupyion shape on the performance of enhanced tubes with the separation and reattachment mechanism. Page 8.

[10] BergmanT.L., Lavine A.S., Incropera F.P. and Dewitt D.P., 2011. *Fundamentals of heat and mass transfe, 7th edition.* John Wiley & Sons, USA. Pages 14, 538, 542.

[11] Yaghoubi M. and M. Akbari Moosavi. 2014. Three dimensional thermal expansion analysis of an absorber tube in a parabolic trough collector. Pages 1-2.

[12] Bejan A. 2003. *Convection heat transfer*. Wiley, USA.